ACS APPLIED MATERIALS & INTERFACES

www.acsami.org

Research Article

Galunisertib-Loaded Gelatin Methacryloyl Hydrogel Microneedle Patch for Cardiac Repair after Myocardial Infarction

Haiting Chen,[¶] Lu Fan,[¶] Ningxin Peng,[¶] Yong Yin, Dan Mu, Jun Wang,* Ran Meng,* and Jun Xie*

Cite This: *ACS Appl. Mater. Interfaces* 2022, 14, 40491−40500

Read Online

ACCESS | Metrics & More | Article Recommendations | Supporting Information

ABSTRACT: Uncontrolled and excessive fibrosis after myocardial infarction (MI) in the peri-infarct zone leads to left ventricular remodeling and deterioration of cardiac function. Inhibiting fibroblast activation during the mature phase of cardiac repair improves cardiac remodeling and function after MI. Here, we engineered a biocompatible microneedle (MN) patch using gelatin methacryloyl and loaded it with galunisertib, a transforming growth factor-beta (TGF-β)-specific inhibitor, to treat excessive cardiac fibrosis after MI. The MN patch could sustainably release galunisertib for more than 2 weeks and provide mechanical support for the fragile ventricular wall. After being applied to a rat model of MI, the galunisertib-loaded MN patch improved long-term cardiac function and reduced cardiac fibrosis by effectively inhibiting TGF-β depending on fibroblast activation. This strategy shows the potential of the MN patch as an advanced platform to locally deliver direct antifibrotic drugs to prevent myocardial fibrosis for the treatment of MI and the promotion of cardiac repair.

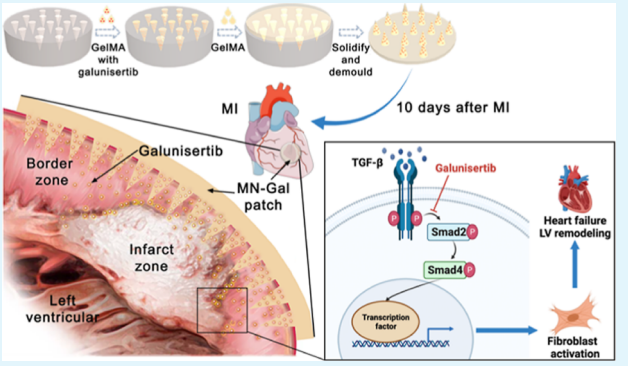

KEYWORDS: *myocardial infarction, heart failure, cardiac fibrosis, microneedle patch, galunisertib*

INTRODUCTION

Myocardial infarction (MI) is a leading cause of morbidity and mortality worldwide.[1] Even after complete revascularization and intensive medication therapy, the 10 year all-cause mortality rate of patients with heart failure (HF) after MI remains high at 58.9%.[2] In the pathological process of HF after MI, ventricular remodeling plays a vital role and is characterized histologically by myocardial hypertrophy, apoptosis, and fibrosis.[3] Although the initial reparative fibrosis is crucial for cardiac healing, fibrotic expansion in the peri-infarct zone and adverse ventricular remodeling during the mature stage of the cardiac repair are major causes of HF after MI.[4] Therefore, effective and manipulatable antifibrotic therapy is a potential therapeutic target in the clinical treatment of HF after MI.

The drugs currently used clinically to prevent ventricular remodeling, such as beta-blockers, angiotensin-converting enzyme inhibitors, and angiotensin receptor blockers, can only partially and indirectly inhibit fibrosis.[5] Myocardial fibrosis is inevitable in most patients even after intensive medication therapy.[6] Transforming growth factor-beta (TGF-β) plays a crucial role in cardiac fibroblast transdifferentiation and extracellular matrix deposition.[7] Galunisertib, a small-molecular inhibitor of TGF-β receptor I kinase that specifically downregulates the phosphorylation of Smad2, can be an ideal antifibrotic drug and has been used to treat cancer and liver, lung, and kidney fibrosis.[8]

However, broad inhibition of TGF-β was observed to be failed in the treatment of cardiac fibrosis after MI because of the increased risk of cardiac rupture.[9] As extracellular matrix deposition is the physiological process of scar formation after MI,[10] traditional antifibrotic drug treatment is harmful to scar formation and ventricular wall stability. Hence, exploring the drug platform which could deliver galunisertib locally and maintain the ventricular wall's stability would help develop a new therapeutic strategy to attenuate cardiac fibrosis in the peri-infarct zone.

Recently, biocompatible microneedles (MNs) emerged as an advanced technology platform for local drug delivery and sustained drug release.[11] MNs can penetrate through the transdermal layer to access the inner tissues in a minimally invasive way and have been applied to treat wound healing and neuropathic pain.[12] On the other hand, MNs could be used as a biocompatible patch on the injured heart to provide mechanical support and prevent cardiac rupture. Therefore, it is conceivable that the employment of a galunisertib-loaded MN patch to injured myocardium would provide a distinctive

Received: March 26, 2022
Accepted: July 25, 2022
Published: August 29, 2022

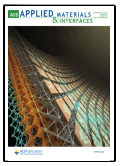

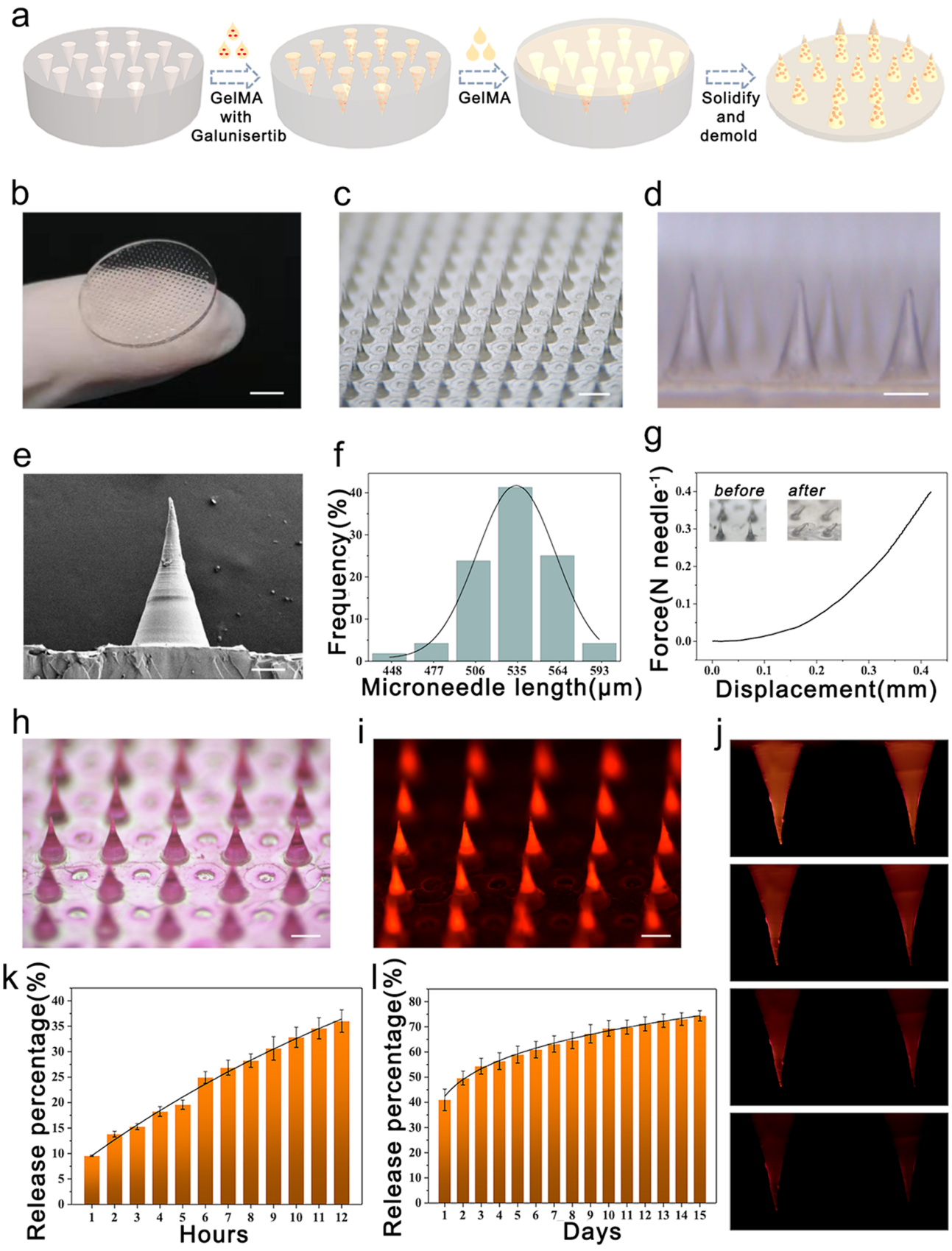

Figure 1. Characterization of the galunisertib-loaded GelMA MN patch. (a) Schematic diagram of the fabrication of MN patches. (b) Digital photo of the whole MN patch; scale bar: 4 mm. (c–d) Microscopic images of MNs; scale bars: 600 μm in (c) and 260 μm in (d). (e) SEM image of a single MN; scale bar: 100 μm. (f) Uniformity statistics of MNs. (g) Compressive mechanical performance of MN patches. (h–i) Optical and fluorescence microscopic images of the MN patch loaded with Rhodamine B; scale bars: 300 μm. (j) Fluorescence photographs of the release status of MNs; scale bar: 150 μm. (k–l) Accumulative Rhodamine B release percentage from MNs in the first 12 h (k) and next 15 days (l).

https://doi.org/10.1021/acsami.2c05352
ACS Appl. Mater. Interfaces 2022, 14, 40491–40500

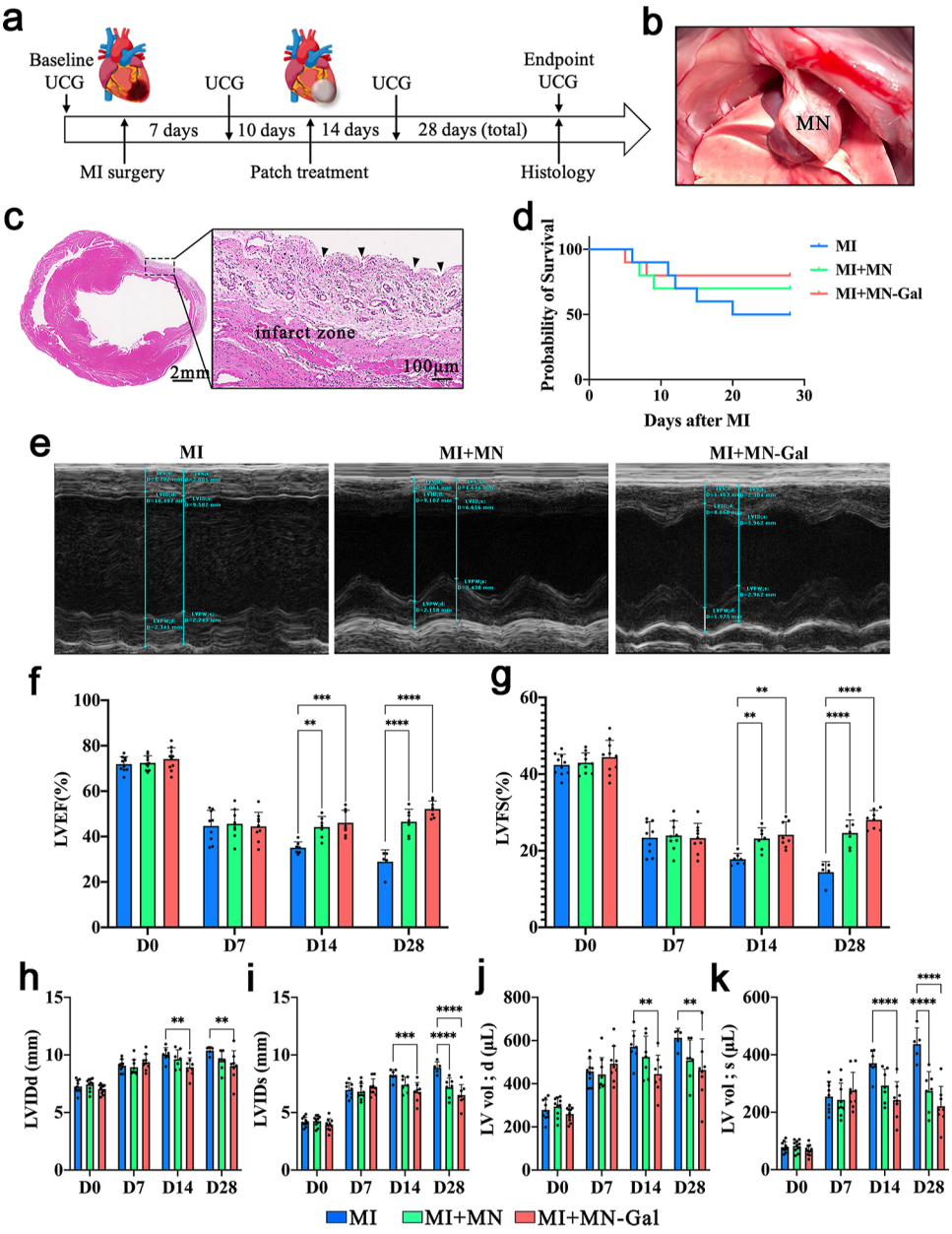

Figure 2. MN-Gal patch preserved the cardiac structure and function following MI. (a) Schematic showing the overall animal study design used to test the therapeutic benefits of MN-Gal patch in a rat model of MI. (b) Placement of an MN patch on the rat heart. (c) H&E staining indicates the MN pinholes (black arrow) on the infarcted and peri-infarct zone of the infarcted heart (scale bars: 2 mm, left; 100 μm, right). (d) Survival curve of MN-Gal patch-treated MI rats compared with that of blank MN patch-treated MI rats and only MI rats. (e) Representative M-mode echocardiographic image showing the LV wall motion of the hearts 28 days after MI. Diastolic and systolic cycles were analyzed for each image, and three images for each time point were analyzed per rat. (f–k) LVEF, LVFS, LV internal dimension at end-diastole (LVID; d) and end-systole (LVID; s), and LV volume at end-diastole (LV Vol; d) and end-systole (LV Vol; s) were measured by echocardiography before MI surgery (baseline) and 7, 14, and 28 days (endpoint) after MI. $n \geq 5$ animals per group. All data were presented as means ± SD. Comparisons between three groups were performed using two-way ANOVA, followed by Tukey's multiple comparison test. $^{**}P < 0.01$; $^{****}P < 0.0001$ between each group and every other group.

strategy for local and minimally invasive drug delivery to treat cardiac fibrosis.

This study engineered an MN patch with galunisertib loaded into the tips (MN-Gal patch) to deliver the myocardium-targeted drug. Gelatin methacryloyl (GelMA) was chosen as the MN and backing layer material because of its superior biocompatibility, biodegradation, controllable mechanical strength and drug release.[11] In a rat model of MI, we chose to cover the infarct and peri-infarct zones with the MN-Gal patch 10 days after MI when the scar had matured. Notably, the MN-Gal patch sustainedly released loaded galunisertib to effectively inhibit TGF-β signaling locally, contributing to the attenuation of cardiac fibrosis and hypertrophy and improvement of cardiac function. We expect that the MN-Gal patch could be a promising candidate for the treatment of MI and has great clinical significance for improving the long-term outcomes of MI patients.

https://doi.org/10.1021/acsami.2c05352
ACS Appl. Mater. Interfaces 2022, 14, 40491−40500

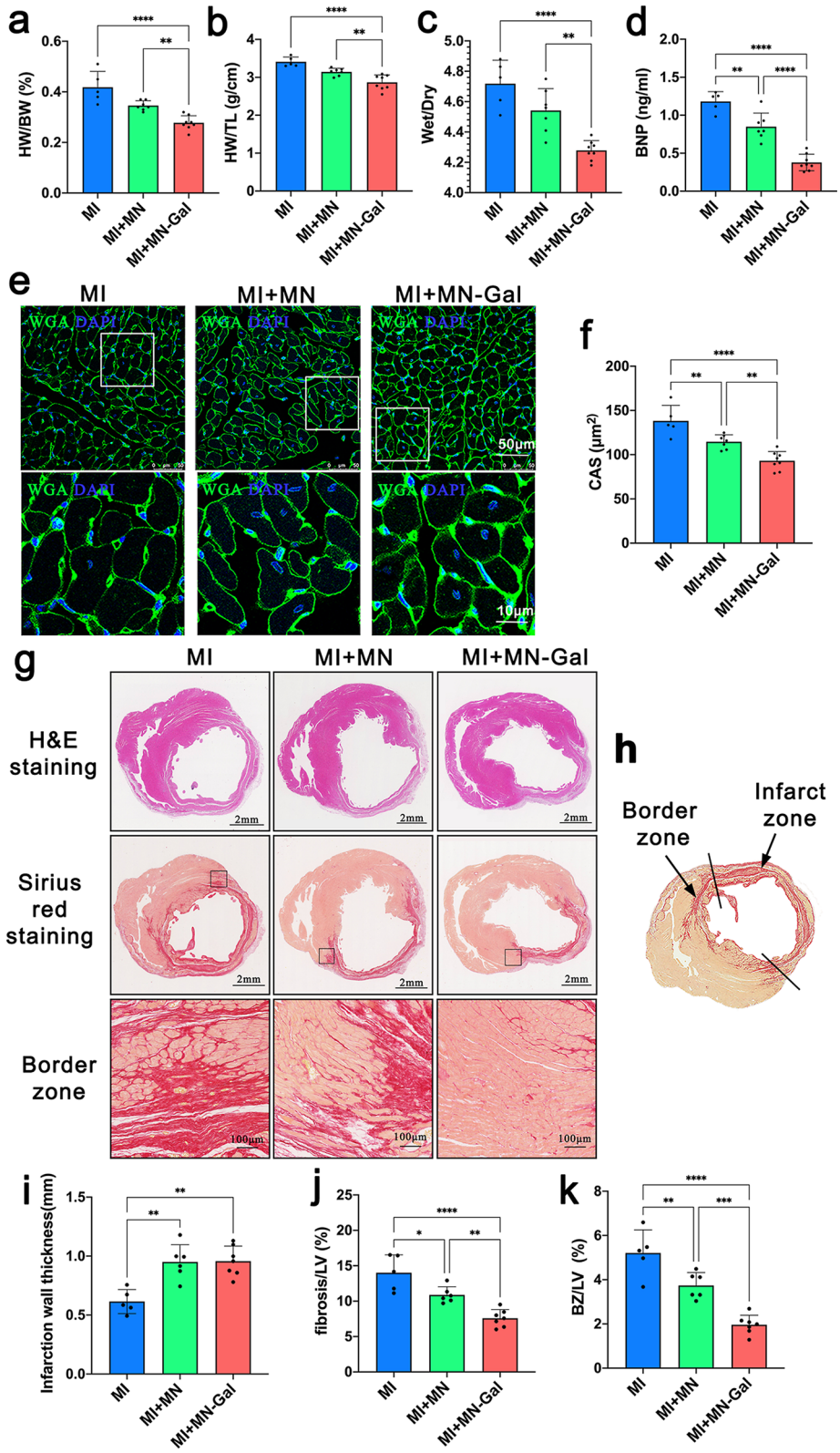

Figure 3. MN-Gal patch decreased infarct scar extension and expansion and protected from myocardial hypertrophy in a rat model of MI. (a–c) HW/BW ratio, HW/BW ratio, and lung wet/dry weight ratio on 28 days after MI. (d) Plasma BNP level at the endpoint. (e) Representative images of WGA staining (scale bars: 50 μm (upper) and 10 μm (lower). (f) CAS shows the relative cardiomyocyte size. $n \geq 5$ animals per group. (g) H&E-stained and Sirius red-stained images of the heart tissue were collected at the endpoint (scale bar: 2 mm and 100 μm). (h) Schematic image revealed the definition of BZ and infarcted zone of a rat model of MI. The BZ area was defined as the total fibrotic area minus the infarct zone area in which LV thickness became thinner. (i) Infarction wall thickness, (j) fibrosis area to LV area ratio, and (k) BZ area to LV area ratio were measured from Sirius red-stained image. $n \geq 5$ animals per group. All data were presented as means ± SD. Comparisons between three groups were performed using one-way ANOVA, followed by Tukey's multiple comparison test. *$P < 0.05$; **$P < 0.01$; ***$P < 0.001$; ****$P < 0.0001$ between each group and every other group.

https://doi.org/10.1021/acsami.2c05352
ACS Appl. Mater. Interfaces 2022, 14, 40491–40500

RESULTS AND DISCUSSION

Characterization of the Galunisertib-Loaded GelMA MN Patch. In a typical experiment, GelMA hydrogel was chosen as an ideal MN tip material due to its high compatibility and bioactivity.[13] Gelatin and synthesized GelMA were dissolved in D2O, and the structure was analyzed by proton nuclear magnetic resonance (1H NMR) (Figure S1). According to the 1H NMR spectra of GelMA, methacryloyl groups successfully replaced the lysine group of gelatin to achieve a 96% degree of substitution. Galunisertib was loaded inside the tips and was then covered by the backing GelMA layer. The galunisertib-loaded GelMA MN patch was fabricated using a two-step template method, as shown in Figure 1a. In the first step, the MN template mold made with polydimethylsiloxane (PDMS) was filled with the solution of tip material by centrifugation and then crosslinked by UV irradiation to solidify the tips. In the second step, the same concentration of GelMA solution was added as the backing layer to cover the tips, solidified, and dried at 37 °C. The MN patch was obtained by demolding. The microstructure of the MN tips was further characterized, as shown in Figure 1b−f. The MN patch was demonstrated to be naturally bent into an arc during the drying process (Figure 1b), which may benefit its fitting to the heart surface during the treatment. Furthermore, all the MN tips were aligned in order in a sharp conical shape (Figure 1c−d). A total of 385 MNs were arranged in a uniform circular shape with a diameter of 17.5 mm. The scanning electron microscopic (SEM) image of a single MN tip confirmed that a single needle tip's height and bottom diameter were about 570 and 260 μm, respectively (Figure 1e−f).

Next, we investigated the mechanical strength of the MNs, which is an essential parameter deciding the ability of the MNs to penetrate the myocardium.[14] For this purpose, the MN patch with a 385 circular array was placed horizontally in a fixed station, and a force sensor was slowly approaching the tips. The measurement started when the sensor touched the tips and ended when it went down by 0.3 mm. The results showed that the MNs had a mechanical strength of ∼0.4 N per needle (Figure 1g), which was reported strong enough for sufficient myocardium penetration without breaking.[15] Another advantage of using GelMA as the tip material is that GelMA is a hydrophilic porous material, absorbing interstitial fluids and blood when applied to the heart.[16] Simultaneously, swelling of the MNs may facilitate the release of the payloads after penetrating the myocardium, enhance the interaction of the MNs with the inserted cavity, and immobilize the MN tips inside the punctured site.[17] To examine the drug loading and subsequent release behavior from the GelMA MNs, we used the fluorescent molecule Rhodamine B as the model drug and loaded it into the MNs.[18] The fluorescent images in Figure 1h−i showed the even distribution of Rhodamine B in the MNs. Then, the Rhodamine B-loaded GelMA MN patch was immersed in phosphate-buffered saline (PBS), and the concentration of released Rhodamine B in the PBS was quantified. Figure 1j revealed a gradual decrease of the fluorescence signal from the MNs over time. Quantitative results from Figure 1k−l demonstrated that loaded Rhodamine B could be sustainedly released from the GelMA MNs for at least 15 days.

Taken together, these results demonstrated that the fabricated GelMA MN patch had appropriate tip size and mechanical strength for myocardium penetration and could sustainedly release sufficient loaded drug within a long treatment period.

MN-Gal Patch Preserved Cardiac Structure and Function Following MI. To investigate the practical therapeutic effect of the MN-Gal patch, we applied the MN-Gal patch to a rat model of MI and received different treatments, as shown in Figure 2a. Male Sprague-Dawley rats were divided into three groups and underwent MI surgery by ligating the left anterior descending (LAD) artery.[19] The two groups of model rats receiving patch treatment underwent a second thoracotomy 10 days after MI when traditionally the cardiac repair entered the mature stage and fibrous scar had matured. Blank MN and MN-Gal patches were immobilized onto the epicardial surface of the infarcted and peri-infarcted zone; four echocardiogram examinations (UCG) were recorded during the whole process. At the endpoint, the heart of each rat was harvested for further pathological and molecular biological tests. As shown in Figure 2b, the MN patch was immobile onto the epicardial throughout the 28-day treatment after being attached and did not cause obvious local connective tissue wrapping. Hematoxylin−eosin (H&E) staining of the infarct zone in Figure 2c clearly showed the corresponding pinholes from MN tips penetrating the myocardium tissue, which agrees with the previous result showing the MN patch with enough mechanical strength for myocardium penetration.

According to the survival curve shown in Figure 2d, among all the rats who suffered MI surgery, 50% (5/10) of the MI group, 30% (3/10) of the MI + MN group, and 20% (2/10) of the MI + MN-Gal group died before euthanasia. After dissection, we observed that in the inflammatory phase (1−3 days after MI) and proliferative phase (4−10 days after MI) of cardiac repair, all the rats (three in the MI group, three in the MI + MN group, and two in the MI + MN-gal group) died of cardiac rupture. In the mature phase (more than 10 days after MI), one of the rats in the MI group died of cardiac rupture while the other did not. No deaths occurred in the MI + MN and MI + MN-Gal groups after the MN patches were applied, indicating that the employment of MN patches could prolong the survival period. The cardiac ultrasound images at 28 days after MI are shown in Figure 2e. The statistics of essential parameters reflecting the cardiac function are shown in Figure 2f−k. After MI, the cardiac function of rats in all groups showed a progressive decline. No statistical differences were seen among the three groups, indicating that the severity of MI was similar among rats in different groups before the MN patch was applied. After 10 days of MI, when the MN patch had been treated, the left ventricular ejection fraction (LVEF) and left ventricular fractional shortening (LVFS) of rats in the MI + MN and MI + MN-Gal group no longer decreased and showed an upward trend compared with only the MI group. However, the parameters showed no difference in whether galunisertib was loaded.

MN-Gal Patch Decreased Infarct Scar Extension and Expansion and Protected from Myocardial Hypertrophy in a Rat Model of MI. Heart weight (HW), body weight (BW), lung wet weight and dry weight, and tibia length (TL) were determined, and HW/BW, HW/TL, and lung wet/dry weight ratio (the primary morphometric measures of myocardial hypertrophy) were calculated.[20] As shown in Figure 3a−c, cardiac hypertrophy improved significantly after the treatment of the MN-Gal patch compared with the

https://doi.org/10.1021/acsami.2c05352
ACS Appl. Mater. Interfaces 2022, 14, 40491−40500

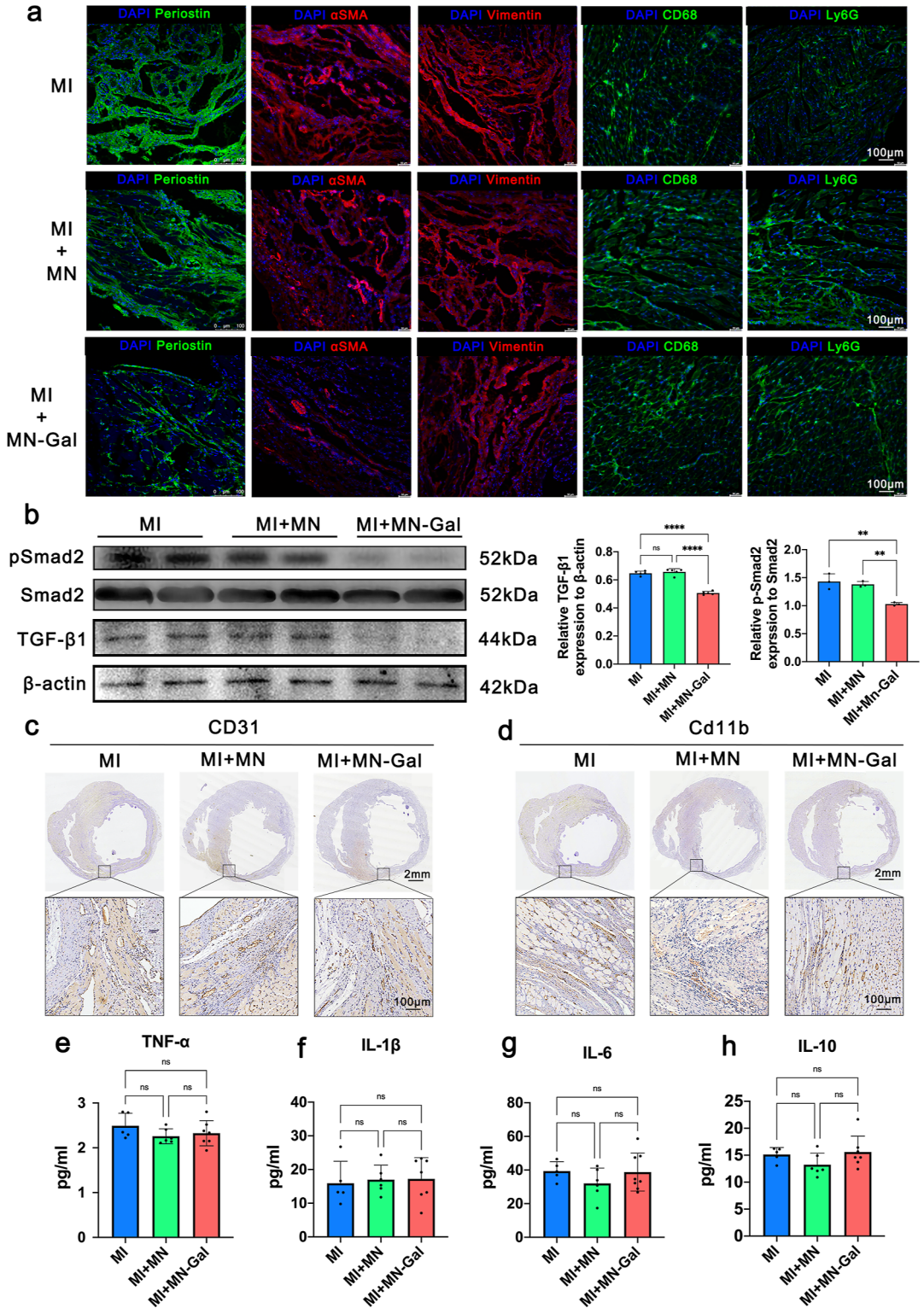

Figure 4. MN-Gal patch prevented fibroblast activation by inhibiting TGF-β/Smad2 signaling but had no apparent effect on angiogenesis and inflammation. (a) Representative IF images of activated fibroblasts stained for periostin (green, row 1) and αSMA (red, row 2), total fibroblasts stained for vimentin (red, row 3), macrophages stained for CD68 (green, row 4), and neutrophils stained for Ly6G (green, row 5). The nuclei were stained for DAPI (blue), scale bar: 100 μm. (b)TGF-β, Smad2, phosphorylated Smad2 (p-Smad2), and β-actin protein expression in rat myocardium at the endpoint were examined by western blot. Quantification of the relative TGF-β/β-actin ratio and p-Smad2/Smad2 ratio. (c) Representative IHC images of angiogenesis stained for CD31 [scale bars: 2 mm (upper) and 100 μm (lower)]. (d) Representative IHC images of inflammatory cell infiltration stained for CD11b [scale bars: 2 mm (upper) and 100 μm (lower)]. (e–h) Myocardium cytokine levels of TNF-α, IL-1β, IL-6, and IL-10 were examined by enzyme-linked immune sorbent assay. $n \geq 5$ animals per group. All data were presented as means ± SD. Comparisons between three groups were performed using one-way ANOVA, followed by Tukey's multiple comparison test. $^{**}P < 0.01$; $^{***}P < 0.001$; $^{****}P < 0.0001$ between each group and every other group.

https://doi.org/10.1021/acsami.2c05352
ACS Appl. Mater. Interfaces 2022, 14, 40491−40500

untreated MI group or blank MN patch-treated group. Plasma brain natriuretic peptide (BNP), a parameter directly associated with the severity of HF,[21] was also significantly lower in the MI + MN-Gal group than in the untreated MI or MI + MN group (Figure 3d). To further investigate the amelioration of cardiac hypertrophy by the MN-Gal patch, 4′,6-diamidino-2-phenylindole (DAPI), and wheat germ agglutinin (WGA) staining were applied to identify cardiomyocytes (Figure 3e). Similarly, quantitative results of cardiomyocyte cross-sectional area (CAS) showed that the blank MN patch could decrease the CAS, while loading galunisertib in the patch further resulted in a significant decrease in the CAS (Figure 3f).

Infarct size and cardiac fibrosis were assessed by H&E staining and Sirius red staining shown in Figure 3g. Infarct size was calculated as a percentage of the circumflexion length of the LV-free wall, and infarct wall thickness was calculated as a percentage of the thickness of the septal wall. The schematic image of Sirius red staining in Figure 3h showed the definition of the peri-infarct zone/border zone (BZ) as the total area of fibrosis minus the infarct zone area in which LV thickness became thinner.[22] The infarct wall thickness increased in both MI + MN and MI + MN-Gal groups (Figure 3i), which may be related to the mechanical support effect of the MN patch. Furthermore, fibrosis area, BZ area, and LV area were determined, and fibrosis/LV and BZ/LV ratios were calculated to evaluate fibrosis degree in the peri-infarct zone.[23] As shown in Figure 3j−k, there was a significant decrease in the MI + MN group compared with the untreated MI group. Similarly, a further decline was seen after treating the MN-Gal patch, indicating the reduction of the proportion of fibrosis and BZ area in the LV area. All these results suggest that the delivery of galunisertib to the myocardium mediated by the MN patch could effectively attenuate cardiac fibrosis in the peri-infarct area and myocardial hypertrophy after MI.

MN-Gal Patch Prevented Fibroblast Activation by Inhibiting TGF-β/Smad2 Signaling but Had No Apparent Effect on Angiogenesis and Inflammation. Periostin, a matricellular protein, is highly expressed in activated fibroblasts after MI and plays a vital role in the pathology of cardiac hypertrophy and fibrosis.[24] Periostin is required in the TGF-β signaling during the cardiac repair of MI.[25] Hence, immunofluorescence (IF) staining was applied, and an apparent decrease of periostin$^+$ cells was observed in MN-Gal patch-treated MI hearts compared to untreated and blank MN patch-treated MI hearts (Figure 4a), indicating the suppression of fibroblast activation. αSMA is a marker for myofibroblasts and vascular smooth muscle cells. In the peri-infarct zone, except for vascular smooth muscle cells, αSMA$^+$ myofibroblasts were markedly reduced in the cardiac interstitium after MN-Gal patch treatment, whereas a large number of αSMA$^+$ myofibroblasts were seen in the cardiac interstitium in the MI group and the group using blank MN patches. Vimentin IF staining suggested that the total fibroblast population in the cardiac interstitium was not significantly altered in these three groups, suggesting that galunisertib was released into the infarct myocardium and inhibited fibroblast activation and transdifferentiation into myofibroblasts without affecting the total fibroblast population. Galunisertib specifically inhibits TGF-β signaling by downregulating the phosphorylation of Samd2.[26] As shown in Figure 4b, the relative protein expression level of TGF-β to β-actin and the phosphorylation of Smad2 decreased significantly in hearts treated with MN-Gal patch compared with those with no treatment or treated with blank MN patch, indicating that the GelMA MN patch could effectively locally release sufficient galunisertib to inhibit TGF-β signaling in the infarcted myocardium.

We also assessed angiogenesis and inflammation under the treatment of the MN patch. The CD31 immunohistochemistry (IHC) staining (Figure 4c) showed that both the blank and galunisertib-loaded MN patches did not impair angiogenesis in the peri-infarct zone. Similarly, CD11b IHC staining (Figure 4d) showed no increased signs of inflammatory cell infiltration after the patch treatment. CD68 and Ly6G IF staining suggested that the use of MN patches did not result in increased macrophage and neutrophil infiltration (Figure 4a). Meanwhile, proinflammatory cytokines (e.g., TNF-α, IL-1β, and IL-6) and suppressive cytokines (e.g., IL-10) were not significantly increased in myocardial tissue (Figure 4e−h). These results suggest that neither the blank MN patch nor the MN-Gal patch could impair angiogenesis or aggravate inflammation during the myocardium repair process.

The blood samples were collected to evaluate further the toxicity of released galunisertib and the MN patch material. No significant changes in serum alanine transaminase (ALT), aspartate transaminase (AST), blood urea nitrogen (BUN), and creatinine (Cr) levels after MN-Gal patch application suggested that targeted cardiac release of galunisertib did not cause liver and kidney damage (Figure S2). Then, the main organs, including lung, liver, kidney, and spleen, were harvested and stained with H&E. The results showed no noticeable histological changes (Figure S3), indicating no apparent systemic toxicity. Moreover, DAPI and terminal deoxynucleotidyl transferase dUTP nick end labeling (TUNEL) staining (Figure S4) of the infarcted hearts showed that applying the MN-Gal patch did not increase cardiomyocyte apoptosis. These results demonstrated that the MN-Gal patch could effectively inhibit TGF-β signaling locally in the infarct and peri-infarct zone, preventing fibrosis expansion into the peri-infarct area, while no significant contribution to the promotion of angiogenesis and antiinflammation was observed.

CONCLUSIONS

In summary, we prepared a biocompatible MN patch for sustained drug delivery to the site of the injured myocardium for MI treatment. HF after MI is a significant cause of morbidity and mortality worldwide.[27] Fibrous scarring is essential for maintaining the stability of the ventricular wall. However, fibrotic expansion in the peri-infarct zone and adverse ventricular remodeling during the mature stage of the cardiac repair are major causes of HF after MI.[28] It is a pity that there is currently no effective therapeutic strategy for inhibiting myocardial fibrosis. The currently used antifibrotic drugs are not effective enough to inhibit cardiac fibrosis. Direct antifibrotic drug treatment is harmful to scar formation and ventricular wall stability and may increase the risk of heart rupture. Also, there is still a lack of innovative platforms that can accurately deliver these drugs to the injured myocardium in a minimally invasive way.

To satisfy these needs, we developed a galunisertib-loaded GelMA MN patch that provided mechanical support and realized local drug therapy in the infarcted myocardium. The drug-release properties can be controlled by adjusting the degree of crosslinking to ensure sustained release for at least 15 days after application. In addition, the MN-Gal patch could

https://doi.org/10.1021/acsami.2c05352
ACS Appl. Mater. Interfaces 2022, 14, 40491−40500

provide mechanical support to restrain adverse LV remodeling and reduce the risk of cardiac rapture. In a rat model of MI, the MN-Gal patch successfully delivered TGF-β-specific inhibitor galunisertib to the infarcted myocardium and effectively inhibited TGF-β/Smad2 signaling, contributing to reduced cardiac fibrosis, protecting from myocardial hypertrophy, and improved cardiac output.

METHOD SECTION

Preparation of GelMA. GelMA hydrogel was obtained from methacrylic modification of gelatin. First, 10 g of gelatin (Sigma-Aldrich, 73865) was added to 100 mL of PBS solution and continuously stirred at 60 °C until it completely dissolved. Second, 10 mL of methacrylic anhydride (Sigma-Aldrich, 276685) was added into gelatin solution drop by drop under stirring and heated at 60 °C for 2 h. Then, preheated PBS buffer (60 °C) was added and continued stirring for 1−2 h. After that, the resultant solution was poured into the dialysis bag, followed by dialysis at 60 °C for 7 days to remove excess methacrylic anhydride. Finally, GelMA was obtained after freeze-drying and stored at −20 °C for standby. Furthermore, gelatin and synthesized GelMA were dissolved in D2O and the structure was analyzed by proton nuclear magnetic resonance (1H NMR) spectroscopy.

Preparation of Galunisertib-Loaded GelMA MNs. 1500 mg/mL Galunisertib (Sigma-Aldrich, SML2851) was mixed in 30 wt % GelMA prepolymer and 1 vol % 2-hydroxy-2-methylpropiophenone (Sigma-Aldrich, 405655) solution, and then dropped into negative PDMS mold (385 conical arrays, whose diameter is 17.5 mm, conical length is 570 μm, and basal diameter is 260 μm). Afterward, the air in conical MN cavities was removed by centrifugation, and the mixed solution was stuffed into the cavities. The composite prepolymer MN solution was solidified by UV light (365 nm). Then, 0.3 mg/mL GelMA prepolymer solution without galunisertib was added into the mold as the backing solution and solidified in the same way. Finally, the galunisertib-loaded GelMA MN patch was obtained by drying and carefully demolded.

Mechanical Properties of the MN Patch. The resultant GelMA MN patches (tips faced up) were put on the fixed platform of the force analyzing system (ZHIQU Co. Ltd., Guangzhou, China). The force sensor gradually closed to the MN patch and began to test once it touched the tips. It traveled at 0.2 mm/s speed and stopped at the displacement of 0.4 mm. The morphology of MNs before and after the test was characterized using an optical microscope.

Drug Release Profile of the MN-Gal Patch. Rhodamine B (Hefei BASF Biotechnology Company, LR0441) was encapsulated in GelMA MN patch tips. Then, the whole patches were immersed in PBS solution at room temperature. In the first 12 h, the PBS solution was taken out every hour. The fluorescence intensity was measured in the microplate reader. Then, the same volume of fresh PBS solution was added. After that, the fluorescence intensity was measured every other day for the next 15 days. During the whole process, the fluorescence intensity of Rhodamine B in GelMA MNs was recorded using a fluorescence microscope.

Animal Procedures. All procedures with animals were approved by the Institutional Ethics Committee of Nanjing Drum Tower Hospital (Approval no. 20201015) and performed following the guidelines outlined in the Guide for the Care and Use of Laboratory Animals published by the National Institutes of Health (Eighth Edition). Male Sprague−Dawley rats (n = 30, weighing 200−220 g, 6−7 weeks) were obtained from the Beijing SPF biotechnology company. Six rats were housed per cage under standard conditions (temperature, 22−24 °C; humidity, 50 ± 5%; and light, from 8 a.m. to 8 p.m.) and allowed access to food and water ad libitum. After a 7 day acclimation period, the rats were anesthetized with pentobarbital and connected to a ventilator. LAD ligation was performed through the fourth intercostal space, and the proximal LAD was ligated with 6−0 sutures. Successful MI was confirmed by a pale area below the suture sites and the following echocardiography assessment. The animals were randomly subjected to three treatment groups: MI rat without treatment group (MI, n = 10), MI rat with blank GelMA MN patch treatment group (MI + MN, n = 10), and MI rat with galunisertib-loaded GelMA MN patch treatment group (MI + MN-Gal, n = 10). In the MI + MN and MI + MN-Gal groups, the GelMA MN patches were applied to cover the epicardial surface of the infarct and peri-infarct zone 10 days after MI when the scar had matured. Echocardiography was performed five times throughout the experiment procedure to determine the cardiac function. Serum and plasma were collected through the abdominal aorta when the rats were euthanized. Plasma BNP levels were measured using commercially available enzyme-linked immunoassay kits (Abcam, ab108816). The serum activities of ALT, AST, BUN, and Cr were measured using the commercial reagent kits (Nanjing Jiancheng Bioengineering Institute, C009-2-1, C010-2-1, C013-2-1, C011-2-1). The hearts of all rats were harvested and apportioned for H&E staining, Picrosirius red staining (Abcam, ab150681), IHC staining, IF staining, WGA staining (Sigma-Aldrich, L4895), and TUNEL staining (Roche, 11684795910). For IF staining, the periostin antibody (Abcam, ab14041), α-SMA antibody (Cell Signaling Technology, 48938), Vimentin antibody (AIFang biological, AF20105), CD68 antibody (Abcam, ab53444), and Ly6G antibody (Abcam, ab25377) were detected with the antirabbit Alexa Fluor488 antibody (Jackson immunoresearch, 111-545-144), antimouse Cy3 antibody (Invitrogen, A10521), and antirat Alexa Flour488 antibody (Jackson immunoresearch, 112-545-167). For IHC staining, the CD31 antibody (Abcam, ab182981) and CD11b antibody (Abcam, ab133357) were used. Livers, spleens, lungs, and kidneys were also harvested for H&E staining. Total protein from myocardial tissues in the infarct and peri-infarct zone was extracted. The target protein level was examined by western blot with primary antibodies against TGF-β1 (Abcam, ab215715), Smad2 (Cell Signaling Technology, 5339), phosphor-Smad2 (Cell Signaling Technology, 18338), and β-Actin (Cell Signaling Technology 4970). Myocardium cytokines TNF-α, IL-1β, IL-6, and IL-10 were measured using commercially available enzyme-linked immunoassay kits (MULTI SCIENCES, EK382/3, EK301B/3, EK306/3, and EK310/2).

Statistical Analysis. Data from at least five independent experiments were presented as mean ± SD unless otherwise indicated. Data were tested using either a two-tailed, unpaired student's t-test or one-way analysis of variance (ANOVA), followed by Tukey's multiple comparison test to determine differences between groups at a single timepoint. Data were tested using two-way ANOVA, followed by Bonferroni's multiple comparison test to determine differences between groups at multiple time points. All analyses were performed using Prism 6 software (GraphPad), and only differences with

https://doi.org/10.1021/acsami.2c05352
ACS Appl. Mater. Interfaces 2022, 14, 40491−40500

a P value of less than 0.05 were considered statistically significant.

■ ASSOCIATED CONTENT

Supporting Information

The Supporting Information is available free of charge at https://pubs.acs.org/doi/10.1021/acsami.2c05352.

Additional experimental data including the NMR spectra of GelMA and gelatin ;serum ALT, AST, Scr, and BUN; H&E staining image of lung, liver, kidney, and spleen tissues; and TUNEL staining of the heart (PDF)

■ AUTHOR INFORMATION

Corresponding Authors

Jun Wang − *Department of Emergency, Nanjing Drum Tower Hospital, The Affiliated Hospital of Nanjing University Medical School, Nanjing University, Nanjing 210008, China*; Phone: 86-25-68182812; Email: wjgaogou@aliyun.com

Ran Meng − *Department of Endocrinology, Nanjing Drum Tower Hospital, The Affiliated Hospital of Nanjing University Medical School, Nanjing University, Nanjing 210008, China*; Phone: 86-25-68182812; Email: mengran-apple@hotmail.com

Jun Xie − *Department of Cardiology, Nanjing Drum Tower Hospital, the Affiliated Hospital of Nanjing University Medical School, Nanjing University, Nanjing 210008, China; Department of Cardiology, Nanjing Drum Tower Hospital, Clinical College of Nanjing Medical University, Nanjing 210008, China*; orcid.org/0000-0002-9385-3242; Phone: 86-25-68182812; Email: xiejun@nju.edu.com

Authors

Haiting Chen − *Department of Cardiology, Nanjing Drum Tower Hospital, the Affiliated Hospital of Nanjing University Medical School, Nanjing University, Nanjing 210008, China*

Lu Fan − *State Key Laboratory of Bioelectronics, School of Biological Science and Medical Engineering, Southeast University, Nanjing 210096, China*

Ningxin Peng − *Department of Cardiology, Nanjing Drum Tower Hospital, Clinical College of Nanjing Medical University, Nanjing 210008, China*

Yong Yin − *Department of Cardiology, Nanjing Drum Tower Hospital, the Affiliated Hospital of Nanjing University Medical School, Nanjing University, Nanjing 210008, China*

Dan Mu − *Department of Radiology, Nanjing Drum Tower Hospital, The Affiliated Hospital of Nanjing University Medical School, Nanjing University, Nanjing 210008, China*

Complete contact information is available at: https://pubs.acs.org/10.1021/acsami.2c05352

Author Contributions

¶H.C., F.L., and N.P. contributed equally to this work.

Notes

The authors declare no competing financial interest.

■ ACKNOWLEDGMENTS

This work was supported by the National Natural Science Foundation of China (grant numbers 81870358 and 92068116); the Key Projects of Science and Technology of Jiangsu Province (grant number BE2019602); the Science Fund for Distinguished Young Scholars in Jiangsu Province (grant number BK20211501); the Fundamental Research Funds for the Central Universities (grant number 14380501); the Jiangsu Provincial Medical Youth Talent (grant number QNRC2016018); and the Key Project supported by the Medical Science and Technology Development Foundation, Nanjing Department of Health (grant number JQX19004).

■ REFERENCES

(1) Clemente-Moragón, A.; Gómez, M.; Villena-Gutiérrez, R.; Lalama, D. V.; García-Prieto, J.; Martínez, F.; Sánchez-Cabo, F.; Fuster, V.; Oliver, E.; Ibáñez, B. Metoprolol Exerts a Non-Class Effect against Ischaemia-Reperfusion Injury by Abrogating Exacerbated Inflammation. *Eur. Heart J.* **2020**, *41*, 4425−4440.

(2) Petrie, M. C.; Jhund, P. S.; She, L.; Adlbrecht, C.; Doenst, T.; Panza, J. A.; Hill, J. A.; Lee, K. L.; Rouleau, J. L.; Prior, D. L.; et al. Ten-Year Outcomes after Coronary Artery Bypass Grafting According to Age in Patients with Heart Failure and Left Ventricular Systolic Dysfunction: An Analysis of the Extended Follow-up of the Stich Trial (Surgical Treatment for Ischemic Heart Failure). *Circulation* **2016**, *134*, 1314−1324.

(3) Frangogiannis, N. G. Pathophysiology of Myocardial Infarction. *Compr. Physiol.* **2015**, *5*, 1841−1875.

(4) Talman, V.; Ruskoaho, H. Cardiac Fibrosis in Myocardial Infarction-from Repair and Remodeling to Regeneration. *Cell Tissue Res.* **2016**, *365*, 563−581.

(5) Hayashi, M.; Tsutamoto, T.; Wada, A.; Tsutsui, T.; Ishii, C.; Ohno, K.; Fujii, M.; Taniguchi, A.; Hamatani, T.; Nozato, Y.; et al. Immediate Administration of Mineralocorticoid Receptor Antagonist Spironolactone Prevents Post-Infarct Left Ventricular Remodeling Associated with Suppression of a Marker of Myocardial Collagen Synthesis in Patients with First Anterior Acute Myocardial Infarction. *Circulation* **2003**, *107*, 2559−2565.

(6) González, A.; Schelbert, E. B.; Díez, J.; Butler, J. Myocardial Interstitial Fibrosis in Heart Failure: Biological and Translational Perspectives. *J. Am. Coll. Cardiol.* **2018**, *71*, 1696−1706.

(7) Hanna, A.; Frangogiannis, N. G. The Role of the Tgf-Beta Superfamily in Myocardial Infarction. *Front. Cardiovasc. Med.* **2019**, *6*, 140.

(8) Holmgaard, R. B.; Schaer, D. A.; Li, Y.; Castaneda, S. P.; Murphy, M. Y.; Xu, X.; Inigo, I.; Dobkin, J.; Manro, J. R.; Iversen, P. W.; et al. Targeting the Tgfbeta Pathway with Galunisertib, a Tgfbetari Small Molecule Inhibitor, Promotes Anti-Tumor Immunity Leading to Durable, Complete Responses, as Monotherapy and in Combination with Checkpoint Blockade. *J Immunother Cancer* **2018**, *6*, 47.

(9) Rainer, P. P.; Hao, S.; Vanhoutte, D.; Lee, D. I.; Koitabashi, N.; Molkentin, J. D.; Kass, D. A. Cardiomyocyte-Specific Transforming Growth Factor Beta Suppression Blocks Neutrophil Infiltration, Augments Multiple Cytoprotective Cascades, and Reduces Early Mortality after Myocardial Infarction. *Circ. Res.* **2014**, *114*, 1246−1257.

(10) Frangogiannis, N. G. The Extracellular Matrix in Myocardial Injury, Repair, and Remodeling. *J. Clin. Invest.* **2017**, *127*, 1600−1612.

(11) Luo, Z.; Sun, W.; Fang, J.; Lee, K.; Li, S.; Gu, Z.; Dokmeci, M. R.; Khademhosseini, A. Biodegradable Gelatin Methacryloyl Microneedles for Transdermal Drug Delivery. *Adv. Healthcare Mater.* **2019**, *8*, 1801054.

(12) Chi, J.; Zhang, X.; Chen, C.; Shao, C.; Zhao, Y.; Wang, Y. Antibacterial and Angiogenic Chitosan Microneedle Array Patch for Promoting Wound Healing. *Bioact. Mater.* **2020**, *5*, 253−259.

(13) Yue, K.; Trujillo-de Santiago, G.; Alvarez, M. M.; Tamayol, A.; Annabi, N.; Khademhosseini, A. Synthesis, Properties, and Biomedical Applications of Gelatin Methacryloyl (Gelma) Hydrogels. *Biomaterials* **2015**, *73*, 254−271.

(14) Prausnitz, M. R. Engineering Microneedle Patches for Vaccination and Drug Delivery to Skin. *Annu. Rev. Chem. Biomol. Eng.* **2017**, *8*, 177−200.

(15) Tang, J.; Wang, J.; Huang, K.; Ye, Y.; Su, T.; Qiao, L.; Hensley, M. T.; Caranasos, T. G.; Zhang, J.; Gu, Z.; et al. Cardiac Cell-

Integrated Microneedle Patch for Treating Myocardial Infarction. *Sci. Adv.* **2018**, *4*, No. eaat9365.
(16) Lim, S.; Park, T. Y.; Jeon, E. Y.; Joo, K. I.; Cha, H. J. Double-Layered Adhesive Microneedle Bandage Based on Biofunctionalized Mussel Protein for Cardiac Tissue Regeneration. *Biomaterials* **2021**, *278*, 121171.
(17) Zhu, J.; Zhou, X.; Kim, H. J.; Qu, M.; Jiang, X.; Lee, K.; Ren, L.; Wu, Q.; Wang, C.; Zhu, X.; et al. Gelatin Methacryloyl Microneedle Patches for Minimally Invasive Extraction of Skin Interstitial Fluid. *Small* **2020**, *16*, 1905910.
(18) Sun, H.; Chen, J.; Han, X.; Liu, H. Multi-Responsive Hydrogels with Ucst- and Lcst-Induced Shrinking and Controlled Release Behaviors of Rhodamine B. *Mater. Sci. Eng., C* **2018**, *82*, 284−290.
(19) Sciarretta, S.; Yee, D.; Nagarajan, N.; Bianchi, F.; Saito, T.; Valenti, V.; Tong, M.; Del Re, D. P.; Vecchione, C.; Schirone, L.; et al. Trehalose-Induced Activation of Autophagy Improves Cardiac Remodeling after Myocardial Infarction. *J. Am. Coll. Cardiol.* **2018**, *71*, 1999−2010.
(20) Baartscheer, A.; Schumacher, C. A.; Vanborren, M. M.; Belterman, C. N.; Coronel, R.; Opthof, T.; Fiolet, J. W. Chronic Inhibition of Na+/H+-Exchanger Attenuates Cardiac Hypertrophy and Prevents Cellular Remodeling in Heart Failure. *Cardiovasc. Res.* **2005**, *65*, 83−92.
(21) Ambrosy, A. P.; Braunwald, E.; Morrow, D. A.; DeVore, A. D.; McCague, K.; Meng, X.; Duffy, C. I.; Rocha, R.; Velazquez, E. J.; Investigators, P.-H. Angiotensin Receptor-Neprilysin Inhibition Based on History of Heart Failure and Use of Renin-Angiotensin System Antagonists. *J. Am. Coll. Cardiol.* **2020**, *76*, 1034−1048.
(22) Arbustini, E.; Kramer, C. M.; Narula, J. Arrhythmogenic Potential of Border Zone after Myocardial Infarction: Scar Is More Than Just a Healed Wound. *JACC Cardiovasc. Imaging* **2018**, *11*, 573−576.
(23) Snider, J. C.; Riley, L. A.; Mallory, N. T.; Bersi, M. R.; Umbarkar, P.; Gautam, R.; Zhang, Q.; Mahadevan-Jansen, A.; Hatzopoulos, A. K.; Maroteaux, L.; et al. Targeting 5-Ht2b Receptor Signaling Prevents Border Zone Expansion and Improves Microstructural Remodeling after Myocardial Infarction. *Circulation* **2021**, *143*, 1317−1330.
(24) Oka, T.; Xu, J.; Kaiser, R. A.; Melendez, J.; Hambleton, M.; Sargent, M. A.; Lorts, A.; Brunskill, E. W.; Dorn, G. W., 2nd; Conway, S. J.; et al. Genetic Manipulation of Periostin Expression Reveals a Role in Cardiac Hypertrophy and Ventricular Remodeling. *Circ. Res.* **2007**, *101*, 313−321.
(25) Snider, P.; Hinton, R. B.; Moreno-Rodriguez, R. A.; Wang, J.; Rogers, R.; Lindsley, A.; Li, F.; Ingram, D. A.; Menick, D.; Field, L.; et al. Periostin Is Required for Maturation and Extracellular Matrix Stabilization of Noncardiomyocyte Lineages of the Heart. *Circ. Res.* **2008**, *102*, 752−760.
(26) Tran, H. C.; Wan, Z.; Sheard, M. A.; Sun, J.; Jackson, J. R.; Malvar, J.; Xu, Y.; Wang, L.; Sposto, R.; Kim, E. S.; et al. Tgfbetar1 Blockade with Galunisertib (Ly2157299) Enhances Anti-Neuroblastoma Activity of the Anti-Gd2 Antibody Dinutuximab (Ch14.18) with Natural Killer Cells. *Clin. Cancer Res.* **2017**, *23*, 804−813.
(27) Shih, H.; Lee, B.; Lee, R. J.; Boyle, A. J. The Aging Heart and Post-Infarction Left Ventricular Remodeling. *J. Am. Coll. Cardiol.* **2011**, *57*, 9−17.
(28) Paik, D. T.; Rai, M.; Ryzhov, S.; Sanders, L. N.; Aisagbonhi, O.; Funke, M. J.; Feoktistov, I.; Hatzopoulos, A. K. Wnt10b Gain-of-Function Improves Cardiac Repair by Arteriole Formation and Attenuation of Fibrosis. *Circ. Res.* **2015**, *117*, 804−816.

https://doi.org/10.1021/acsami.2c05352
ACS Appl. Mater. Interfaces 2022, 14, 40491−40500